Optimized Quantification of Translocator Protein Radioligand ^{18}F-DPA-714 Uptake in the Brain of Genotyped Healthy Volunteers

Sonia Lavisse[1,2], Daniel García-Lorenzo[3,4], Marie-Anne Peyronneau[5], Benedetta Bodini[3–6], Claire Thiriez[1,2,7], Bertrand Kuhnast[5], Claude Comtat[5], Philippe Remy*[1,2,7,8], Bruno Stankoff*[3,4], and Michel Bottlaender[5,9]

[1]CEA-DSV-I2BM, MIRCen, Fontenay-aux-Roses, France; [2]CNRS-UMR9199, Universités Paris-Sud and Paris-Saclay, Fontenay-aux-Roses, France; [3]Institut du Cerveau et de la Moelle épinière, Inserm-U1127 and Sorbonne University, UPMC-UMRS-1127, Paris, France; [4]CNRS-UMR7225, Paris, France; [5]CEA-DSV-I2BM, SHFJ and IMIV, UMR1023 Inserm/CEA/Paris-Sud University, Orsay, France; [6]Department of Neuroimaging, Institute of Psychiatry, King's College London, London, England; [7]Neurology Department, Centre Expert Parkinson, CHU Henri Mondor, AP-HP, Créteil, France; [8]Paris-Est University, Créteil, France; and [9]CEA-DSV-I2BM, Neurospin, Gif-sur-Yvette, France

Translocator protein (TSPO) is expressed at a low level in healthy brain and is upregulated during inflammatory processes that may occur in neurodegenerative diseases. Thus, TSPO may be a suitable in vivo indicator of neurodegeneration. Here, we quantified the ^{18}F-DPA-714 radioligand in healthy TSPO-genotyped volunteers and developed a method to eliminate the need for invasive arterial blood sampling. **Methods:** Ten controls (7 high-affinity binders [HABs] and 3 mixed-affinity binders [MABs]) underwent ^{18}F-DPA-714 PET with arterial and venous sampling. ^{18}F-DPA-714 binding was quantified with a metabolite-corrected arterial plasma input function, using the 1- and 2-tissue-compartment models (TCMs) as well as the Logan analysis to estimate total volume distribution (V_T) in the regions of interest. Alternative quantification methods were tested, including tissue-to-plasma ratio or population-based input function approaches normalized by late time points of arterial or venous samples. **Results:** The distribution pattern of ^{18}F-DPA-714 was consistent with the known distribution of TSPO in humans, with the thalamus displaying the highest binding and the cerebellum the lowest. The 2-TCM best described the regional kinetics of ^{18}F-DPA-714 in the brain, with good identifiability (percentage coefficient of variation $< 5\%$). For each region of interest, V_T was 47.6% ± 6.3% higher in HABs than in MABs, and estimates from the 2-TCM and the Logan analyses were highly correlated. Equilibrium was reached at 60 min after injection. V_T calculated with alternative methods using arterial samples was strongly and significantly correlated with that calculated by the 2-TCM. Replacement of arterial with venous sampling in these methods led to a significant but lower correlation. **Conclusion:** Genotyping of subjects is a prerequisite for a reliable quantification of ^{18}F-DPA-714 PET images. The 2-TCM and the Logan analyses are accurate methods to estimate ^{18}F-DPA-714 V_T in the human brain of both HAB and MAB individuals. Population-based input function and tissue-to-plasma ratio with a single arterial sample are promising alternatives to classic arterial plasma input function. Substitution with venous samples is promising but still requires methodologic improvements.

Received Feb. 24, 2015; revision accepted May 12, 2015.
For correspondence or reprints contact: Sonia Lavisse, 18 Route du Panorama, 92260 Fontenay-aux-Roses, France.
E-mail: sonia.lavisse@cea.fr
*Contributed equally to this work.
Published online May 29, 2015.

Key Words: PET; ^{18}F-DPA-714; genotyped human; TSPO; quantification

J Nucl Med 2015; 56:1048–1054
DOI: 10.2967/jnumed.115.156083

Neuroinflammation is implicated in many neurodegenerative diseases and microglial activation is suspected to play a role in the central nervous system (*1*). The identification of a PET radiotracer that can detect the microglial activation could prove to be a useful noninvasive approach to facilitate the characterization and understanding of neurodegeneration.

The translocator protein (TSPO) (18 kDa), which is located in the outer mitochondrial membrane, is widely distributed in many peripheral tissues and in the central nervous system (*2*). The abundance of TSPO is low in normal brain tissue but is markedly elevated in neuroinflammatory brain diseases. TSPO is thus considered a promising target for the early imaging of microglial activation. The ^{11}C-PK11195 ligand was the first described TSPO radioligand and has been extensively used in animal models and in patients with neurodegenerative diseases over the past 2 decades. Nevertheless, this ligand has many limitations, including strong nonspecific and plasma protein binding and low brain uptake. A second generation of TSPO radioligands with improved properties has since been developed, including ^{11}C-PBR28 ([methyl-^{11}C]*N*-acetyl-*N*-(2-methoxybenzyl)-2-phenoxy-5-pyridinamine), ^{18}F-PBR111 (2-(6-chloro-2-(4-(3-^{18}F-fluoropropoxy)phenyl)imidazo[1,2-a]pyridin-3-yl)-*N,N*-diethylacetamide), ^{18}F-FEDAA1106 (*N*-(5-fluoro-2-phenoxyphenyl)-*N*-(2-^{18}F-fluoroethyl-5-methoxybenzyl)acetamide), ^{18}F-FEPPA (*N*-2-(2-^{18}F-fluoroethoxy)benzyl-*N*-(4-phenoxypyridin-3-yl)acetamide), ^{18}F-PBR06 (*N*-(2,5-dimethoxybenzyl)-2-^{18}F-fluoro-*N*-(2-phenoxyphenyl)acetamide), ^{11}C-DPA-713 (*N,N*-diethyl-2-[2-(4-^{11}C-methoxyphenyl)-5,7-dimethyl-pyrazolo[1,5-a]pyrimidin-3-yl]-acetamide), and ^{18}F-DPA-714 (*N,N*-diethyl-2-(2-(4-(2-^{18}F-fluoroethoxy)phenyl)-5,7-dimethylpyrazolo[1,5-*a*]pyrimidin-3-yl)acetamide). Although some ligands radiolabeled with ^{11}C are highly specific for TSPO, with many advantages over the ^{11}C-PK11195, their short half-life considerably complicates their widespread use.

Among the ^{18}F-labeled compounds, ^{18}F-FEDAA1106 has showed slow kinetics in healthy individuals and Alzheimer disease patients (*3*) not suitable for in vivo imaging and quantification of TSPO. ^{18}F-PBR06 (*4*) demonstrated favorable properties in healthy humans but produced brain-penetrant radiolabeled metabolites that could bias the binding quantification. ^{18}F-FEPPA and ^{18}F-PBR111 displayed favorable properties for imaging in healthy humans (*5,6*), although ^{18}F-FEPPA is rapidly metabolized.

Recent preclinical studies (*7–9*) have identified ^{18}F-DPA-714 as a promising TSPO ligand for in vivo imaging, and ^{18}F-DPA-714 has been used to quantify TSPOs in healthy subjects (*10*) and in amyotrophic lateral sclerosis, Alzheimer, or stroke patients (*11–13*). In most studies, quantification was performed without arterial samples or metabolite analysis and was based either on a simplified compartmental model (the cerebellum as a reference region (*10,12*)) or on a cluster analysis (*10,11,13*).

Interestingly, Owen et al. (*14*) demonstrated in humans that second-generation TSPO tracers target 2 binding sites that lead to 3 affinity patterns: high-, low-, and mixed-affinity binders (HABs, LABs, and MABs, respectively). The recent TSPO radioligands, therefore, have to be evaluated by accounting for the TSPO genotype of each subject, which has not been the case so far for ^{18}F-DPA-714.

Here, we evaluated the ability of ^{18}F-DPA-714 to quantify the TSPO in the brain of 10 healthy subjects with known TSPO genotype. Using arterial blood sampling and metabolite correction, we sought to determine the compartmental model that best described ^{18}F-DPA-714 cerebral uptake. We investigated whether the total distribution volume (V_T) could be properly identified and differed as a function of the TSPO genotype. We determined the scan duration needed for stable V_T estimates. Last, we studied whether a population-based input function (PBIF) method or the use of venous sampling could provide accurate quantification while avoiding the need for invasive arterial blood sampling.

MATERIALS AND METHODS

Study Design

Ten healthy volunteers (4 women and 6 men; age ± SD, 43.5 ± 15.7 y) were included. Written informed consent was obtained from all participants. All individuals were genotyped for the rs6971 polymorphism within the TSPO gene, and genetic analysis revealed 7 HABs and 3 MABs. Each participant underwent T1-weighted MR imaging (to delineate anatomic boundaries for region-of-interest [ROI] analysis) and ^{18}F-DPA-714 PET scanning. A ^{18}F-DPA-714 bolus was injected intravenously (201.4 ± 26.3 MBq), and the dynamic PET acquisition lasted 90 min. During acquisition, sequential arterial and venous blood was sampled to generate an arterial input function (AIF) and venous input function.

Supplemental data (available at http://jnm.snmjournals.org) provide details on volunteers, genetic analysis procedure, ^{18}F-DPA-714 synthesis, and imaging protocols.

^{18}F-DPA-714 PET Quantification

Reconstructed dynamic data were realigned for motion correction according to the process of frame-to-reference image registration in Pmod (version 3.5; PMOD Technologies Ltd.).

All T1 MR images were automatically segmented using Freesurfer 5.3, which is documented and freely available for download online (http://surfer.nmr.mgh.harvard.edu/). Selected segmented ROIs were those described as having a moderate, low, or high density of TSPO in normal conditions (*15*): thalamus; caudate; putamen; hippocampus; white matter; cerebellum; and occipital, parietal, frontal, and temporal cortices. Data from left and right regions were averaged.

After coregistration (BrainVISA), the MR imaging–defined ROIs were applied to the dynamic PET scan to derive regional time–activity curves.

The 1- and 2-tissue-compartment model (1-TCM and 2-TCM, respectively) were applied to the dynamic PET data (Pmod). Blood volume correction was fixed at 5%. The outcome parameters V_T, V_s (specific volume of distribution), and kinetic rate constants were estimated for each region. Logan graphical analysis was tested with the fit starting at 30 min.

To investigate the scanning duration required for reproducible estimates of V_T, a time-stability analysis was performed (2-TCM) by analyzing reduced scan durations ranging from 90 ($V_{T\text{-}90\ min}$) to 30 min, with a 10-min step.

To simplify the quantification, the equilibrium state between the parent plasma P and the free ligand F compartments (and between free F and bound B ligand compartments) was estimated from the ratio of the concentrations in these 2 compartments (F/P and B/F) in the 2-TCM. At equilibrium, the ratio of brain tissue to AIF ($ratio_{AIF}$) corresponds to the definition of the V_T parameter and is proportional to the receptor density (*16*). From equilibrium, these ratios were individually calculated and were compared with the corresponding V_T extracted from 2-TCM analysis ($V_{T\text{-}2TCM}$).

The equivalence between unchanged ^{18}F-DPA-714 concentrations in venous and arterial plasma was also tested for each individual. At equivalence, the ratio obtained between the brain tissue and the unchanged venous plasma activity concentrations was calculated ($ratio_{vein}$) and compared with $V_{T\text{-}2TCM}$.

More details on ^{18}F-DPA-714 PET data quantification and PBIF method are described in the supplemental data.

PBIF

We used a leave-one-out approach based on all subjects: for each subject, a standard input function (SIF) was created by averaging the AIF of the 9 other subjects. The SIF was then normalized by the value of the individual AIF at time T_α ($AIF_{T\alpha}$) so that the SIF was dimensionless.

To replace the arterial sample with the venous samples for the normalization of the SIF, we defined a linear function f(x) to estimate the value of AIF at time T_α based on venous samples. To evaluate the accuracy of the PBIF method, V_T was assessed with the Logan graphical model using as input the original AIF ($V_{T\text{-}Logan}$), the arterial-based input function ($V_{T\text{-}PBIF\text{-}AIF}$), or the venous-based input function ($V_{T\text{-}PBIF\text{-}vein}$).

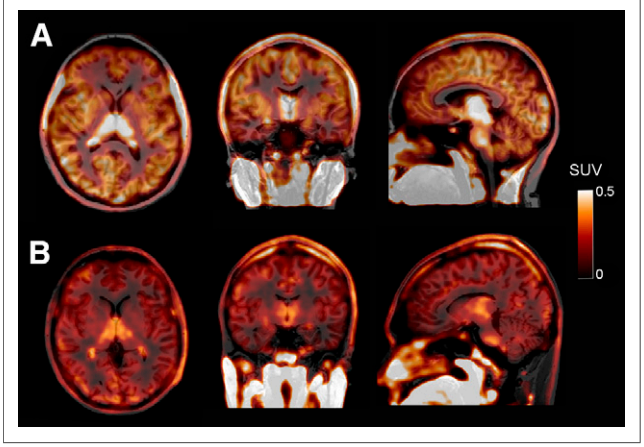

FIGURE 1. ^{18}F-DPA-714 representative SUV PET images (summed from 60 to 90 min) showing axial, sagittal, and coronal views of HAB (A) and MAB (B) individual.

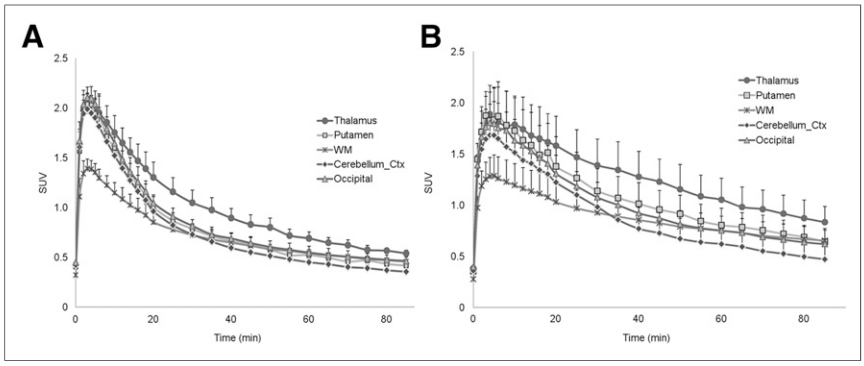

FIGURE 2. Time–activity-curves of SUV expressed as mean ± SD in several brain structures of MAB (A) and HAB (B) subjects.

Statistical Analysis

Data are presented as the mean ± SD. Goodness of fit by the nonlinear least-squares method was evaluated using the Akaike information criterion (AIC). The SE of estimation was expressed as a percentage of the rate constant (coefficient of variation [%COV]). AIC estimates from the 1- and 2-TCM were compared with a Wilcoxon paired *t* test for each ROI. V_T values between MABs and HABs were compared using a Mann–Whitney *U* test. Coefficients of correlation (Spearman) were evaluated between the different parameters. Statistical analysis was conducted with R (R Project for Statistical Computing). The threshold of significance was set to a *P* value of less than 0.05.

RESULTS

^{18}F-DPA-714 Distribution

All subjects showed fairly uniform ^{18}F-DPA-714 binding in the brain, with higher levels of radioactivity in HABs than in MABs (Fig. 1). The thalamus region demonstrated the highest ^{18}F-DPA-714 uptake.

The concentration of the ligand in tissue peaked within the first 4 min and washed out with different elimination rates depending on the genetic group and ROI (Fig. 2). The peak was slightly higher, and washout was faster in MABs than in HABs.

Between 60 and 90 min, the thalamus exhibited the highest washout (mean standardized uptake value [SUV], ~0.75 and ~1.11 for MAB and HAB groups, respectively), followed by the parietal and frontal cortices (~0.63 and ~0.90), the hippocampus, white matter, occipital cortex (~0.59 and ~0.79), putamen (~0.56 and ~0.88) and caudate, cerebellum, and temporal cortex (~0.51 and ~0.69).

In plasma, the metabolism of ^{18}F-DPA-714 was relatively slow, with an unchanged fraction reaching 54.8% ± 9.7% of the total plasma activity at 90 min in arterial samples. Similar values were obtained in the venous plasma with 54.5% ± 9.6% at 90 min. The difference between the venous and arterial unchanged fraction was low in each individual: 3.1% ± 1.8% at 90 min, except for 1 participant who displayed a much higher unchanged fraction in venous plasma (+19%) than in arterial plasma. This individual was excluded from the analysis based on venous data.

After a rapid distribution phase (peak of 7.3 ± 3.2 SUV at 1 min), the unchanged radiotracer in arterial plasma showed slow elimination kinetics with low concentrations and small interindividual variability (0.22 ± 0.08 SUV at 30), with no SUV difference between HABs and MABs (respectively, 0.133 ± 0.037 and 0.137 ± 0.080 between 60 and 90 min).

In venous plasma, the elimination kinetics occurred at the same rate as in arterial plasma, with lower values (24% ± 13%) and higher interindividual variability.

^{18}F-DPA-714 Quantification

The 2-TCM fitted correctly the kinetics of the radiotracer and identified the best AIC scores (33.5 ± 16.5). The V_T parameter was identified with a %COV for $V_{T\text{-}2TCM}$ ranging between 2.1% and 4.9%, depending on the ROI. This model estimated the rate constants with moderate identifiability (mean, 8.2, 19.0, 25.3 and 17.4 %COV for K_1, k_2, k_3, and k_4, respectively).

Fitting with the 1-TCM deviated from the measured PET data (Fig. 3), and this model gave a significantly higher AIC score (49.2 ± 20.7) than the 2-TCM ($P < 0.004$).

Therefore, the unconstrained 2-TCM best described the kinetics of both specific and nonspecific ^{18}F-DPA-714 binding (Table 1).

V_T was higher in HABs (+45.9% ± 4.8%) than MABs, with a trend toward significance in the thalamus and white matter regions ($P = 0.055$) despite the small number of subjects. Figure 4 shows the variability in the V_T estimates, which is substantial in the HAB group. No correlation between the age of subjects and V_T values in the HAB group was found ($-0.2 < r < -0.61$, depending on ROI).

The nondisplaceable distribution volume V_{ND} (K_1/k_2) and V_s ($V_s = V_T - V_{ND}$) were estimated for each region. When both HABs and MABs were considered, V_{ND} estimates ranged from 0.82 mL/cm^3 in the thalamus to 1.13 mL/cm^3 in the caudate, with an average of 0.975 ± 0.08 mL/cm^3 across regions (mean V_{ND} was 0.77 and 1.07 mL/cm^3 in MABs and HABs, respectively). V_{ND} was equal to 1.02 mL/cm^3 across all regions and individuals, using the polymorphism plot method developed by Guo et al. (*5*). For both genetic groups, V_s was lowest in the caudate and highest in the thalamus (Table 2). The ratio of specific to total uptake of ^{18}F-DPA-714 was approximately 80% in the thalamus and the hippocampus regions, approximately 65% in the occipital, parietal, frontal, and temporal cortices, and only 50% in the caudate. This ratio was similar for HABs and MABs.

The time-stability analysis showed that $V_{T\text{-}60\ min}$ was similar to $V_{T\text{-}90\ min}$ ($V_{T\text{-}60\ min} > 98\%$ of the $V_{T\text{-}90\ min}$ value in all ROIs for MABs and HABs), and covariance was stable (+2.29% higher at

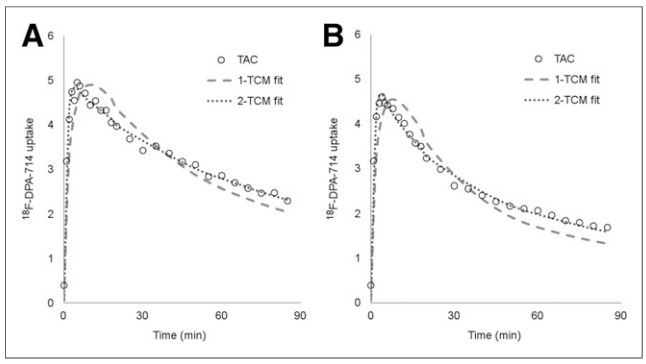

FIGURE 3. Model-fit comparisons. Example of 1- and 2-TCM fit to parietal (A) and occipital cortex (B) for one HAB subject.

TABLE 1
Rate Constant Estimates from 2-TCM Analysis

Region	K_1 (mL·min^{-1}·cm^{-3})		k_2 (min^{-1})		k_3 (min^{-1})		k_4 (min^{-1})	
	MAB	HAB	MAB	HAB	MAB	HAB	MAB	HAB
Thalamus	0.39 (0.12)	0.35 (0.15)	0.77 (0.40)	0.40 (0.14)	0.53 (0.09)	0.28 (0.06)	0.12 (0.05)	0.06 (0.01)
Caudate	0.33 (0.09)	0.24 (0.13)	0.72 (0.38)	0.18 (0.07)	0.49 (0.15)	0.13 (0.07)	0.17 (0.09)	0.08 (0.02)
Putamen	0.35 (0.07)	0.37 (0.21)	0.57 (0.30)	0.39 (0.26)	0.31 (0.20)	0.26 (0.13)	0.08 (0.02)	0.08 (0.02)
Hippocampus	0.29 (0.08)	0.30 (0.22)	0.70 (0.40)	0.55 (0.62)	0.38 (0.23)	0.22 (0.18)	0.15 (0.10)	0.05 (0.03)
White matter	0.23 (0.05)	0.20 (0.10)	0.53 (0.32)	0.22 (0.13)	0.31 (0.14)	0.15 (0.10)	0.10 (0.04)	0.05 (0.01)
Cerebellum	0.39 (0.09)	0.30 (0.17)	0.77 (0.42)	0.32 (0.17)	0.36 (0.24)	0.30 (0.19)	0.29 (0.25)	0.11 (0.05)
Occipital	0.45 (0.13)	0.32 (0.15)	1.03 (0.77)	0.33 (0.13)	0.46 (0.15)	0.27 (0.13)	0.31 (0.29)	0.09 (0.03)
Parietal	0.36 (0.05)	0.33 (0.17)	0.65 (0.15)	0.32 (0.15)	0.52 (0.09)	0.27 (0.13)	0.17 (0.10)	0.08 (0.02)
Frontal	0.40 (0.08)	0.31 (0.17)	0.87 (0.50)	0.25 (0.11)	0.48 (0.16)	0.23 (0.10)	0.18 (0.11)	0.08 (0.02)
Temporal	0.27 (0.09)	0.28 (0.18)	0.44 (0.39)	0.37 (0.31)	0.23 (0.24)	0.26 (0.17)	2.00 (2.56)	0.08 (0.03)

Data in parentheses are SDs.

60 than at 90 min). $V_{T\text{-}60\ min}$ and $V_{T\text{-}90\ min}$ were highly correlated when all subjects were pooled ($r = 0.92$ for the white matter, $r = 0.59$ for the putamen, $r > 0.90$ for other ROIs, $P < 0.001$). When the duration of the scan was reduced to 30 min, V_T identifiability was poorer (%COV > 10) and showed higher bias to $V_{T\text{-}90\ min}$ (Fig. 5).

$V_{T\text{-}Logan}$ values were highly correlated with those obtained with the 2-TCM ($r > 0.98$, $P < 10^{-8}$; Table 2): the mean underestimation of the V_T with this approach was 2.07% and 3.01% over all ROIs for MABs and HABs, respectively.

As a prerequisite of the alternative quantification methods, B/F and F/P were calculated and were found to rapidly increase with time, reaching a plateau at 30 min (Fig. 6) for each subject. They both were stable at 60 min, with a mean variation of 2% between 60 and 90 min for all individuals and ROIs. No difference was observed between HABs and MABs. ^{18}F-DPA-714 therefore reached a true equilibrium after 60 min after injection. The $ratio_{AIF}$ was calculated for the last 30 min (60–90 min) for each individual: it was highly correlated with the $V_{T\text{-}2TCM}$ for all regions ($r = 0.93 \pm 0.05$, $P < 10^{-3}$; Fig. 7) and was 29.9% ± 5.0% higher than the $V_{T\text{-}2TCM}$. The $ratio_{vein}$ was 72.7% ± 6.6% higher than the $V_{T\text{-}2TCM}$ across all ROIs, and both parameters were found correlated as well ($r = 0.83 \pm 0.06$, $P = 0.01$).

In the PBIF method, the correlation between the AIF points and the area under the curve was highest at 40 min ($r = 0.96$, $P < 10^{-5}$). This time point was chosen as T_α to normalize the SIF. $V_{T\text{-}PBIF\text{-}AIF}$ was strongly correlated with $V_{T\text{-}Logan}$ and $V_{T\text{-}2TCM}$ ($r = 0.97 \pm 0.03$, $P = 0.02$; Fig. 7). The difference between $V_{T\text{-}PBIF\text{-}AIF}$ and $V_{T\text{-}Logan}$ values was 2.2% ± 5.8%. $V_{T\text{-}PBIF\text{-}vein}$ and $V_{T\text{-}Logan}$ (difference of 2.4% ± 29.3%) showed a mean correlation of 0.67 ± 0.10, which was significant in the caudate, putamen, thalamus, white matter, and frontal and parietal cortex regions.

DISCUSSION

We quantified ^{18}F-DPA-714 uptake in the brain of TSPO-genotyped healthy individuals.

We found that the 2-TCM described the kinetics of the tracer better than the 1-TCM, with good identifiability of the V_T, V_{ND}, and V_s parameters. Furthermore, the Logan approach was highly correlated with the 2-TCM and accurately estimated V_T. This approach can be further applied at the voxel level to produce parametric V_T maps. Our observations are consistent with studies regarding TSPO radioligands showing that the 2-TCM is superior to the 1-TCM (*5,6,12,17*). The range of our V_T estimates (3–5 mL/cm^3) was similar to that found for ^{18}F-DPA-714 (*12*), ^{11}C-PRB28, and ^{18}F-PBR111 in HABs (*5,15*) and for ^{11}C-DPA-713 (*17*). Our estimates in the ROIs were consistent with the known distribution of TSPO in the human brain and with previous studies on ^{11}C-PK11195, ^{11}C-DPA713, ^{11}C-PBR28, and ^{18}F-FEPPA (*6,15,17,18*): the biodistribution of ^{18}F-DPA-714 was widespread and similar in the different cortical regions, but activity concentration was always higher in the thalamus than in the other cerebral regions.

The mean V_{ND} in the brain was 0.975 mL/cm^3, further confirmed by the polymorphism plot method (*5*). This value was in

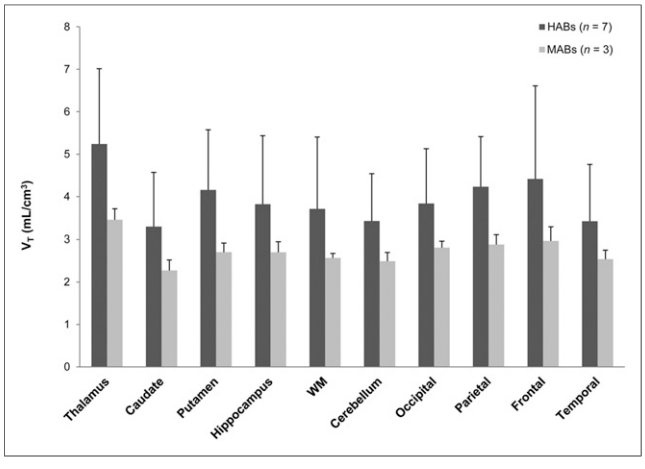

FIGURE 4. V_T estimates in different ROIs for HAB and MAB groups. Data are expressed as mean ± SD.

TABLE 2
V_T, V_s, and BP_{nd} Estimates from 2-TCM and Logan Analysis

Region	2-TCM			Logan, V_T
	V_T	V_s	BP_{nd} (k_3/k_4)	
MAB				
Thalamus	3.45 (0.26)	2.91 (0.35)	5.17 (2.09)	3.43 (0.22)
Caudate	2.27 (0.25)	1.58 (0.47)	3.58 (1.83)	2.35 (0.24)
Putamen	2.70 (0.21)	1.90 (0.59)	3.13 (2.08)	2.74 (0.24)
Hippocampus	2.70 (0.21)	2.20 (0.32)	4.80 (3.12)	2.69 (0.19)
White matter	2.56 (0.22)	1.84 (0.51)	4.33 (2.97)	2.60 (0.24)
Cerebellum	2.49 (0.21)	2.04 (0.22)	3.48 (2.32)	2.49 (0.19)
Occipital	2.81 (0.25)	1.90 (0.68)	4.09 (2.52)	2.87 (0.21)
Parietal	2.88 (0.33)	1.92 (0.68)	3.79 (1.14)	2.89 (0.33)
Frontal	2.97 (0.40)	2.10 (0.72)	4.58 (2.57)	2.97 (0.37)
Temporal	2.54 (0.22)	1.79 (0.45)	2.54 (2.50)	2.53 (0.21)
HAB				
Thalamus	5.24 (1.77)	4.31 (1.48)	4.80 (0.73)	4.84 (1.68)
Caudate	3.30 (1.27)	1.91 (0.76)	1.49 (0.39)	3.05 (1.23)
Putamen	4.17 (1.40)	3.12 (1.21)	3.05 (1.17)	3.95 (1.35)
Hippocampus	3.90 (1.03)	2.90 (1.06)	3.74 (2.18)	3.73 (1.08)
White matter	3.75 (1.13)	2.70 (0.90)	2.80 (1.01)	3.60 (1.14)
Cerebellum	3.44 (1.32)	2.43 (1.23)	2.51 (1.19)	3.24 (1.32)
Occipital	3.86 (1.22)	2.83 (1.00)	2.90 (0.95)	3.72 (1.14)
Parietal	4.24 (1.47)	3.21 (1.31)	3.04 (1.01)	3.98 (1.42)
Frontal	4.43 (1.67)	3.26 (1.39)	2.63 (0.68)	4.12 (1.59)
Temporal	3.43 (1.09)	2.47 (1.08)	2.87 (1.61)	3.28 (1.07)

Data in parentheses are SDs.

the same range as the V_{ND} of the ^{18}F-PBR111 tracer (1.18 mL/cm^3) but was smaller than the V_{ND} of ^{11}C-PRB28 (between 1.6 and 2 (*15*)), indicating that ^{18}F-DPA-714 has lower nonspecific binding than ^{11}C-PRB28. All these data suggest that ^{18}F-DPA-714 is a highly specific ligand for TSPO.

We compared the binding of ^{18}F-DPA-714 in 2 genetic groups using V_T outcome measures. It was not known whether the different binding states reported for ^{11}C-DPA-713 (*19*) also exist for ^{18}F-DPA-714. However, we expected ^{18}F-DPA-714 to exhibit differential affinity for TSPO, as observed for all second-generation TSPO ligands examined to date, because ^{18}F-DPA-714 and ^{11}C-DPA-713 are structurally similar (*20*). We found approximately 50% difference in V_T between HABs and MABs, which was higher than the difference seen with the ^{18}F-FEPPA tracer (between 15% and 30% (*21*)) but within the same range as the one with ^{11}C-PBR28 (*15*).

The difference in V_T between HABs and MABs was evident from the shape of the time–activity curves in each affinity group. In addition, one LAB individual was also initially included in our study, and the corresponding time–activity curve clearly differed from the time–activity curves of the other 2 groups, suggesting that the V_T parameter of LABs is different from that of HABs and MABs (Supplemental Fig. 1). Arterial sampling was not performed for this subject.

Our data confirm that ^{18}F-DPA-714 binding is influenced by the Ala147Thr polymorphism of TSPO, demonstrating the need to genotype each subject to stratify analysis and to accurately interpret ^{18}F-DPA-714 binding.

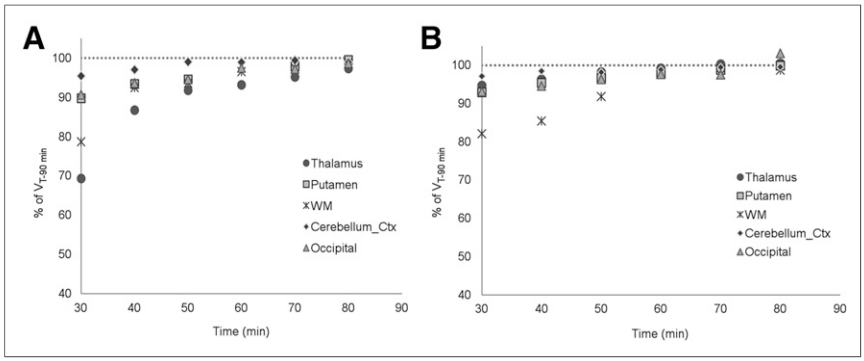

FIGURE 5. V_T time-stability assessment for unconstrained 2-TCM in MAB and HAB groups.

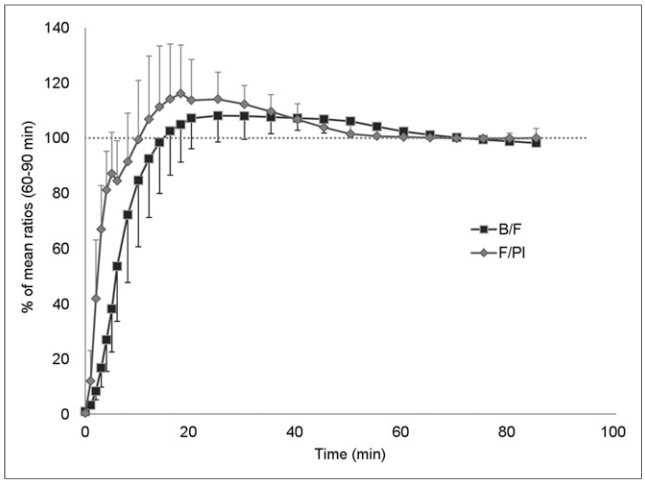

FIGURE 6. Equilibrium assessment showing B/F and F/PI with time. Dotted line represents 100% of mean ratio. Data are expressed as mean ± SD.

In the HABs, V_T showed high variability that could be related to K_1 higher variability in that group, compared with MABs (Table 1). Such variability in HABs has already been reported for other tracers, namely ^{18}F-PBR111 (*5*) and ^{18}F-FEPPA (*22*). As described in Guo et al. (*5*), we checked here if age or injected mass could influence the binding of radiotracers to TSPO but we found no correlation between those variables and ligand binding. This result was consistent with the findings of Suridjan et al. (*21*), who previously determined that age did not influence the binding of the ^{18}F-FEPPA tracer in a large HAB cohort ($n = 22$).

Arterial blood sampling to quantify ^{18}F-DPA-714 is invasive and unsuitable for routine use in patients. Therefore, the reference-based quantitative method (simplified reference tissue model) with the cerebellum as a reference region may be an easier alternative method for data analysis (*10,12*). Although Golla et al. found a good correlation between the binding potential (BP_{nd}) estimated in the simplified reference tissue model and the associated $V_{T\text{-}2TCM}$ values, here we could not always reliably estimate the BP_{nd} parameter using same method. In addition, when correctly estimated, BP_{nd} clearly did not correlate with our $V_{T\text{-}2TCM}$ estimates, likely meaning that V_s in the cerebellum is not negligible and the use of this region as a reference can bias the quantification. Moreover, TSPO is widely distributed in the entire brain, thus no anatomic region can be considered devoid of TSPO binding sites.

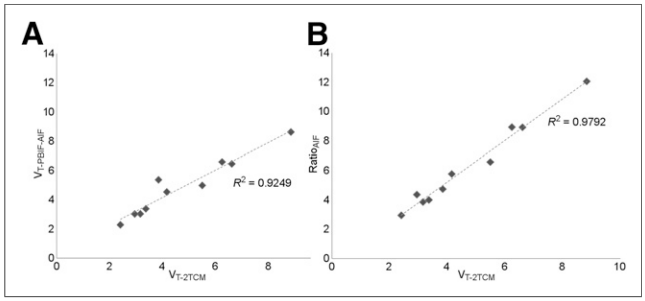

FIGURE 7. Correlations of V_T obtained with 2-TCM and 2 alternative methods: PBIF ($V_{T\text{-}PBIF\text{-}AIF}$) (A) and tissue-to-plasma ratio ($ratio_{AIF}$) (B) for all individuals ($n = 10$).

We tested 3 methods to limit the burden of the ^{18}F-DPA-714 PET scan: (1) we tried to reduce the scan duration and we performed the quantification with (2) venous blood samples only or (3) a single arterial blood sample. Our analyses showed that equilibrium was attained by 60 min, suggesting that acquisition time can be reduced to 60 min in clinical trials. Moreover, the small increase in V_T between 60 and 90 min suggests that radiometabolites potentially entering the brain do not substantially contribute to V_T, as previously described (*23*). Indeed, we recently showed that one ^{18}F-DPA-714 radiometabolite contributes to about 15% of brain radioactivity after 120 min in rats. And this value is likely to be much lower in humans at 90 min because metabolism is much slower in humans than in rodents.

The distribution volume calculated after equilibrium as $ratio_{AIF}$ was strongly correlated with V_T estimated by the 2-TCM. This method could be therefore used with an acquisition starting 60 min after radiopharmaceutical injection and lasting only 30 min. The $ratio_{vein}$ (to avoid using arterial invasive procedure) was correlated with $V_{T\text{-}2TCM}$, but the correlation was high in the same individual while we observed a higher variability between subjects. This finding is probably explained by the variability in the ratio in venous samples between subjects, despite a stable arteriovenous ratio during analysis (60–90 min). Further work is in progress to better understand and to reduce the variability of the venous sampling. Furthermore, although both ratios were correlated with $V_{T\text{-}2TCM}$, they both overestimated the V_T value by approximately 20% and 70%, respectively.

The results of the PBIF method based on one arterial sample or venous samples were highly consistent with those of the full AIF and gave V_T estimates ($V_{T\text{-}PBIF\text{-}AIF}$ and $V_{T\text{-}PBIF\text{-}vein}$) close to the $V_{T\text{-}2TCM}$, with only approximately 2% difference. As expected, the variability of the equilibrium between arterial and vein input functions led to substantial variability in the $PBIF_{vein}$ method (~30% SD for the difference between $V_{T\text{-}PBIF\text{-}vein}$ and $V_{T\text{-}2TCM}$). However, our method based on f(x) minimized the difference between venous and arterial samples and provided a similar error for both $PBIF_{vein}$ and $PBIF_{artery}$ methods. Although this result is encouraging, the number of individuals ($n = 9$) is insufficient to draw definitive conclusions about the utility of a method using only vein sampling. Further work on a larger cohort of HABs and MABs will help us to improve the f(x) function.

CONCLUSION

^{18}F-DPA-714 is highly specific for TSPO and can be quantified using the 2-TCM and the Logan graphical approach. Radiolabeling with ^{18}F renders this ligand suitable for widespread use. It was crucial first to characterize and to quantify this ligand in genotyped healthy controls before using it in patients. Indeed, we showed that ^{18}F-DPA-714 binding is influenced by the TSPO polymorphism, consistent with all second-generation TSPO radioligands. Genotyping subjects should be therefore systematically performed before clinical interpretation of ^{18}F-DPA-714 PET scans in neuroinflammatory studies of various neuropathologies.

DISCLOSURE

The costs of publication of this article were defrayed in part by the payment of page charges. Therefore, and solely to indicate this fact, this article is hereby marked "advertisement" in accordance with

18 USC section 1734. This work was supported by France Parkinson (NCT02319382), ANR-08-MNPS-016-02 (NCT02305264), ANR-10-IAIHU-06, a grant from "Investissement d'Avenir-ANR-11-INBS-0011"—NeurATRIS, CEA, and ECTRIMS. No other potential conflict of interest relevant to this article was reported.

ACKNOWLEDGMENTS

We are grateful to the SHFJ staff and to Irène Buvat for careful reading of the manuscript. We thank Lena Guillot, Isabelle Rebeix, Sylvie Forlani, and Luce Dauphinot for the genetic analysis. We also thank Philippe Gervais and Frédéric Dollé for the qualification of the clinical production.

REFERENCES

1. Glass CK, Saijo K, Winner B, Marchetto MC, Gage FH. Mechanisms underlying inflammation in neurodegeneration. *Cell.* 2010;140:918–934.
2. Venneti S, Lopresti BJ, Wiley CA. The peripheral benzodiazepine receptor (translocator protein 18kDa) in microglia: from pathology to imaging. *Prog Neurobiol.* 2006;80:308–322.
3. Varrone A, Mattsson P, Forsberg A, et al. In vivo imaging of the 18-kDa translocator protein (TSPO) with [^{18}F]FEDAA1106 and PET does not show increased binding in Alzheimer's disease patients. *Eur J Nucl Med Mol Imaging.* 2013;40:921–931.
4. Fujimura Y, Zoghbi SS, Simeon FG, et al. Quantification of translocator protein (18 kDa) in the human brain with PET and a novel radioligand, ^{18}F-PBR06. *J Nucl Med.* 2009;50:1047–1053.
5. Guo Q, Colasanti A, Owen DR, et al. Quantification of the specific translocator protein signal of ^{18}F-PBR111 in healthy humans: a genetic polymorphism effect on in vivo binding. *J Nucl Med.* 2013;54:1915–1923.
6. Rusjan PM, Wilson AA, Bloomfield PM, et al. Quantitation of translocator protein binding in human brain with the novel radioligand [^{18}F]-FEPPA and positron emission tomography. *J Cereb Blood Flow Metab.* 2011;31:1807–1816.
7. Boutin H, Prenant C, Maroy R, et al. [^{18}F]DPA-714: direct comparison with [^{11}C] PK11195 in a model of cerebral ischemia in rats. *PLoS ONE.* 2013;8:e56441.
8. Chauveau F, Van Camp N, Dolle F, et al. Comparative evaluation of the translocator protein radioligands ^{11}C-DPA-713, ^{18}F-DPA-714, and ^{11}C-PK11195 in a rat model of acute neuroinflammation. *J Nucl Med.* 2009;50:468–476.
9. Lavisse S, Guillermier M, Herard AS, et al. Reactive astrocytes overexpress TSPO and are detected by TSPO positron emission tomography imaging. *J Neurosci.* 2012;32:10809–10818.
10. Arlicot N, Vercouillie J, Ribeiro MJ, et al. Initial evaluation in healthy humans of [^{18}F]DPA-714, a potential PET biomarker for neuroinflammation. *Nucl Med Biol.* 2012;39:570–578.
11. Corcia P, Tauber C, Vercoullie J, et al. Molecular imaging of microglial activation in amyotrophic lateral sclerosis. *PLoS ONE.* 2012;7:e52941.
12. Golla SS, Boellaard R, Oikonen V, et al. Quantification of [F]DPA-714 binding in the human brain: initial studies in healthy controls and Alzheimer's disease patients. *J Cereb Blood Flow Metab.* 2015; 35:766–772.
13. Ribeiro MJ, Vercouillie J, Debiais S, et al. Could (18) F-DPA-714 PET imaging be interesting to use in the early post-stroke period? *EJNMMI Res.* 2014;4:28–35.
14. Owen DR, Howell OW, Tang SP, et al. Two binding sites for [^{3}H]PBR28 in human brain: implications for TSPO PET imaging of neuroinflammation. *J Cereb Blood Flow Metab.* 2010;30:1608–1618.
15. Owen DR, Guo Q, Kalk NJ, et al. Determination of [^{11}C]PBR28 binding potential in vivo: a first human TSPO blocking study. *J Cereb Blood Flow Metab.* 2014;34:989–994.
16. Innis RB, Cunningham VJ, Delforge J, et al. Consensus nomenclature for in vivo imaging of reversibly binding radioligands. *J Cereb Blood Flow Metab.* 2007;27:1533–1539.
17. Endres CJ, Pomper MG, James M, et al. Initial evaluation of ^{11}C-DPA-713, a novel TSPO PET ligand, in humans. *J Nucl Med.* 2009;50:1276–1282.
18. Turkheimer FE, Edison P, Pavese N, et al. Reference and target region modeling of [^{11}C]-(R)-PK11195 brain studies. *J Nucl Med.* 2007;48:158–167.
19. Coughlin JM, Wang Y, Ma S, et al. Regional brain distribution of translocator protein using [^{11}C]DPA-713 PET in individuals infected with HIV. *J Neurovirol.* 2014;20:219–232.
20. Owen DR, Gunn RN, Rabiner EA, et al. Mixed-affinity binding in humans with 18-kDa translocator protein ligands. *J Nucl Med.* 2011;52:24–32.
21. Suridjan I, Rusjan PM, Voineskos AN, et al. Neuroinflammation in healthy aging: a PET study using a novel translocator protein 18kDa (TSPO) radioligand, [^{18}F]-FEPPA. *Neuroimage.* 2014;84:868–875.
22. Mizrahi R, Rusjan PM, Kennedy J, et al. Translocator protein (18 kDa) polymorphism (rs6971) explains in-vivo brain binding affinity of the PET radioligand [^{18}F]-FEPPA. *J Cereb Blood Flow Metab.* 2012;32:968–972.
23. Peyronneau MA, Saba W, Goutal S, et al. Metabolism and quantification of [^{18}F] DPA-714, a new TSPO positron emission tomography radioligand. *Drug Metab Dispos.* 2013;41:122–131.